Available online at www.sciencedirect.com
ScienceDirect
Journal of the European Ceramic Society 29 (2009) 1413–1418
www.elsevier.com/locate/jeurceramsoc

Correlations between thermoelectric properties and effective mass caused by lattice distortion in Al-doped ZnO ceramics

J.P. Wiff, Y. Kinemuchi *, H. Kaga, C. Ito, K. Watari

National Institute of Advanced Industrial Science and Technology (AIST), 2266-98 Anagahora, Shimo-Shidami, Moriyama-ku, Nagoya-shi 463-8560, Japan

Received 23 July 2008; received in revised form 16 September 2008; accepted 20 September 2008
Available online 12 November 2008

Abstract

Doped ZnO has practical applications in the industry for thermoelectric generation, owing to its stability at high temperatures. However, the efficiency of energy conversion is not sufficient. In this work, we have focused on an experimental evidence of a first-principles prediction in *ab*-plane tensile strain and the effective mass behavior in ZnO ceramics. The results showed a systematic *c*-axis compression of the lattice up to $c/a = 1.6010$ with increase in the Al additive concentration. It was found that this lattice compression induced an increase in effective mass (m^*) from 0.27 to 0.30 m_0, leading to the enhancement in the Seebeck coefficient normalized by carrier concentration. Besides, both carrier concentration and Hall mobility increased with increase in Al additive concentration. It was concluded that in the ion-doped ZnO system, a high compression of *c*/*a* ratio due to heavy doping could be a key to improving the power factor.

Keywords: Thermoelectric properties; Al-doped ZnO; ZnO; Effective mass

1. Introduction

Thermoelectric materials are promising for enhancing the efficiency in industrial processes owing to the conversion of wasted heat into useful electric energy. In such processes, it is quite common to use temperatures above 500 °C, and in general metal-based thermogenerators are not suitable because they deteriorate in air at high temperature. Thus, oxides like ZnO are very attractive in that application field; however, their efficiency is still quite low ($ZT_{800\,^\circ C} \sim 0.2$).[1]

Usually, the energy conversion efficiency of thermoelectric materials is evaluated in terms of a figure of merit, defined as $ZT = (\alpha^2/\rho\kappa)T$ where α, ρ, κ, and T are Seebeck coefficient, electrical resistivity, thermal conductivity, and absolute temperature, respectively. There are several approaches for increasing the figure of merit, namely, (1) decrease thermal conductivity, (2) decrease electrical resistivity, and (3) increase Seebeck coefficient. Unfortunately, all those parameters are related to each others, for example by carrier concentration, band structures, vacancies, defects, etc.;[2,3] therefore, a highly efficient thermoelectric conversion should be conditioned to an optimum in such variables.

Nevertheless, doping is the most influential factor in determining the electron transport properties; thus, a quantitative understanding of the doping effect is required to enhance the thermoelectric properties. One of the indices of doping is the lattice parameter. In hexagonal structures, as wurtzite-like ZnO, *c*/*a* lattice ratio is a well-known index for characterizing doping effects because *c*/*a* ratio refers to the most energetically stable configuration for a given hexagonal structure even under different loading conditions.[4,5] In a recent work, the effects of biaxial *ab*-plane loadings on band structure, optical transitions, and effective mass of the wurtzite-like ZnO structure were studied by using first-principles density functional calculations.[5] The authors found that in general, *c*/*a* ratio decreases (*c*-axis compression) in a rather linear fashion with the increase in tensile strain in the *ab*-plane of ZnO; also, a slight increase in the effective mass is induced.[5] Unfortunately, the authors did not report experimental evidence about their prediction.

There are some experimental works about the dopant effect in heavily doped ZnO thin films;[6,7] a non-parabolicity in ZnO band structure based on the increment of effective mass as a

* Corresponding author. Tel.: +81 52 736 7157; fax: +81 52 736 7405.
E-mail address: y.kinemuchi@aist.go.jp (Y. Kinemuchi).

0955-2219/$ – see front matter © 2008 Elsevier Ltd. All rights reserved.
doi:10.1016/j.jeurceramsoc.2008.09.014

function of carrier concentration was suggested; however, the effective mass behavior is still unclear, because the contribution of lattice distortion on the effective mass was not considered, as it was predicted by first-principles calculations.[5]

Therefore, this paper is focused on the experimental evidence of first-principles predictions,[5] the case of ZnO lattice distortion caused by dopant and its influence on the lattice structure, effective mass and subsequently thermoelectric behavior.

2. Experimental

2.1. Sample preparation

$Zn_{1-x}Al_xO$ samples with $x = \{0.001, 0.005, 0.01, 0.02, 0.03$ or $0.05\}$ were prepared by solid-state reaction of ZnO (99.8%, Hakusui Tech. Co., Japan) and γ-Al_2O_3 powders (AKP-G015, 99.995%, Sumimoto Chemical, Japan).

Fifty grams of ZnO and Al_2O_3 powders were mixed in stoichiometric quantities in a polyethylene bottle containing 80 ml of ethanol and 130 g of ZrO_2 balls at 100 rpm for 20 h. Afterwards, ethanol and ZrO_2 balls were removed and the slurry was dried under vacuum (∼1 Pa) at 60 °C for 24 h. Dry powders were sieved using a mesh #250.

Samples were compacted in pellets of 5 mm of thickness and 30 mm in diameter. All samples were uniaxially pressed at 30 MPa for 30 s and then hydrostatically cold-pressed at 100 MPa for 1 min. Finally, all samples were sintered in air at 1400 °C for 10 h at a heating rate of 10 °C/min, achieving a density over 99% with respect to their theoretical compositions.

A sample with no Al additive ($x = 0$) was sintered under the same condition with doped ones as a reference for X-ray characterization. The reference sample exhibited a high electrical resistivity; thus no thermoelectrical characterization was performed on it.

2.2. Characterization

All samples were analyzed using an X-ray diffractometer (Rigaku RINT2000, Japan) with Cu anode (Kα) at 40 kV, 200 mA, and step scan of 0.01°. Germanium powder was used as an internal standard for calculating the lattice constants by least-squares method using the XLAT Cell Constant Refinement software.[8]

Before thermoelectrical characterization, all samples were cut in pieces of 5 mm × 5 mm × 14 mm approximately. Afterwards, all faces were polished to ensure a high reproducibility in measurements. Seebeck coefficient and electrical resistivity were measured by static DC method (ULVAC-ZEM-1, Japan) under He atmosphere from room temperature (RT) up to 800 °C and temperature gradients of 20 °C, 30 °C, and 40 °C. All measurements were repeated twice and in both cases, similar values of Seebeck coefficient and electrical resistivity were found, suggesting that at least after short intervals at 800 °C, the samples are chemically and thermally stable. Carrier concentration and Hall mobility were analyzed by DC Hall measurement at RT (Resistest 8300, Toyo-Technica, Japan) under a magnetic field of 0.75 T. Samples had square shape and 10 mm × 10 mm × 0.15 mm in size. Four platinum electrodes were sputtered at the corners of the sample for the Van der Pauw method. In all cases the ohmic behavior at the electrodes was verified, and the Hall voltage was at least two orders of magnitude stronger than noise voltage.

Scanning electron spectroscopy (EDS) was used to characterize the mirror-like polished surface sample before and after treatment at 1250 °C for 40 min in air for thermal etching.

3. Results and discussion

Fig. 1 shows the X-ray diffraction patterns of $Zn_{1-x}Al_xO$ $x = \{0.001, 0.005, 0.01, 0.02, 0.03,$ or $0.05\}$ samples. All samples contain ZnO (JCPDF #75-0576) as the main phase and $ZnAl_2O_4$ (JCPDF # 05-0669) as a minority secondary phase.[9] However, when Al additive concentrations were just 1 at% ($x = 0.01$), then the $ZnAl_2O_4$ diffraction peaks were visible.

Fig. 2a and b show *a* and *c* lattice parameters of $Zn_{1-x}Al_xO$ samples, respectively. In general, lattice parameter *a* tends to increase while *c* tends to decrease with respect to the ZnO standard sample with increasing amount of Al additive. Fig. 3 shows the total distortion of ZnO lattice, estimated from the *c*/*a* lattice ratio, as a function of Al additive concentration. In spite of the scattering in *a* and *c* values, a clear correlation between *c*/*a* ratio and doping concentration is observed.

Shirouzu et al.[10] studied the distribution and solubility limit of Al in sintered ZnO ceramics (0.3 at%), and although their samples were prepared by a colloid method and at a given additive concentration (1 at%), their lattice parameters follow a similar *c*/*a* tendency with those observed in this study: 1.6006 and 1.6020 for doped and undoped samples, respectively.

Fig. 4a shows the surface of a $Zn_{0.999}Al_{0.001}O$ sample after thermal etching at 1250 °C for 40 min. Inset shows a close up on a precipitate located at the grain boundary, both EDS measurements and previous works[10,11] suggest that those precipitates

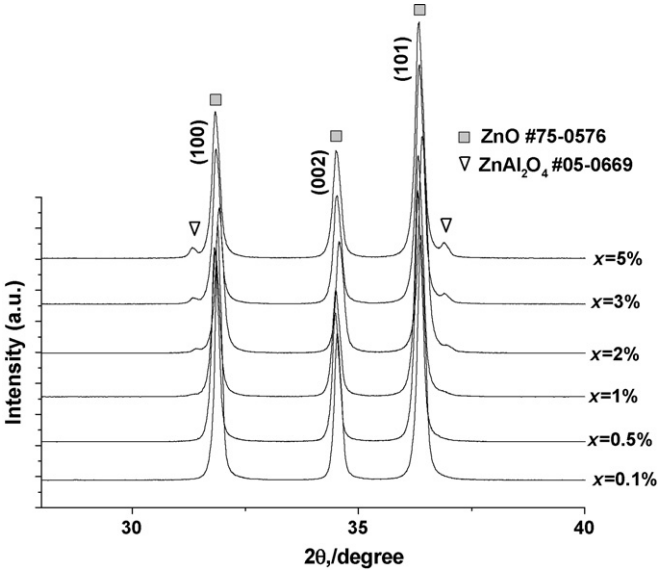

Fig. 1. X-ray diffraction patterns of sintered $Zn_{1-x}Al_xO$ samples with $x = \{0.001, 0.005, 0.01, 0.02, 0.03,$ or $0.05\}$.

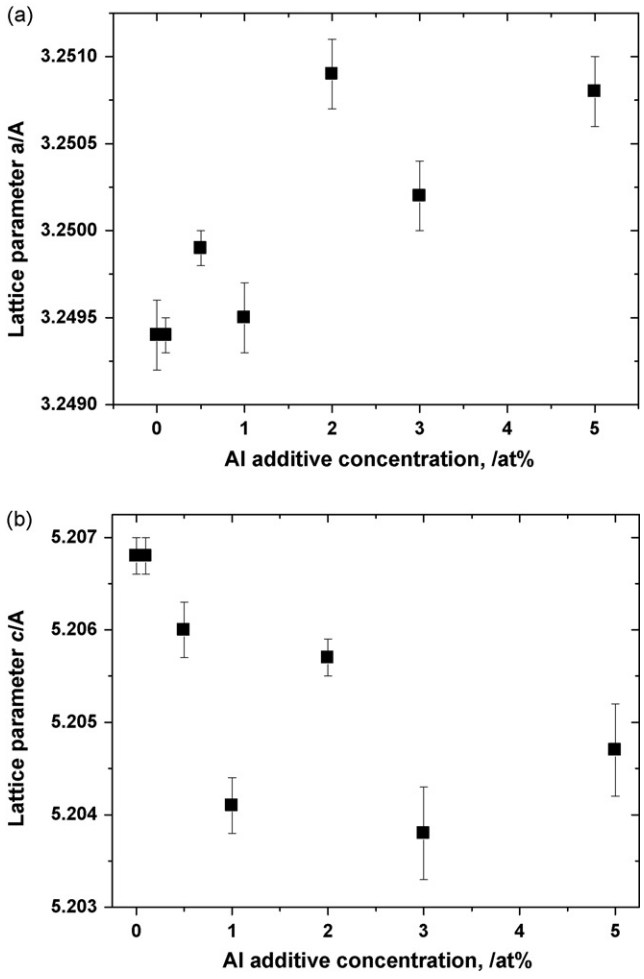

Fig. 2. Tendency of *a* and *c* lattice parameters as a function of Al additive concentration, respectively.

would correspond to a spinel phase. Fig. 4b shows EDS spectra from regions (1) and (2) suggesting that they correspond to an Al-doped ZnO grain (Al content is under the detection limit) and a spinel phase ($ZnAl_2O_4$), respectively. Therefore, Fig. 4 indicates that this sintering method will always produce a spinel phase independent of Al additive concentration probably

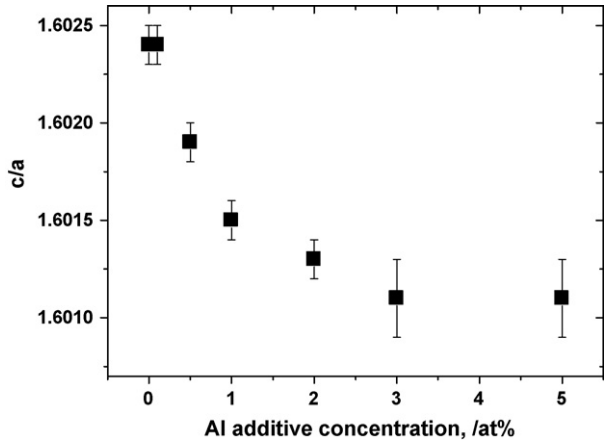

Fig. 3. Variation of the *c*/*a* lattice ratio as a function of Al additive concentration.

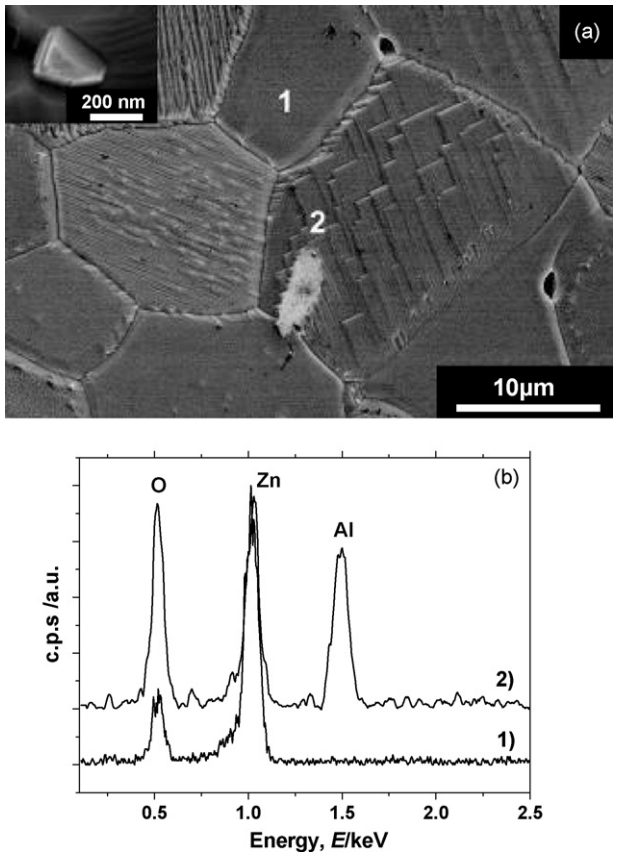

Fig. 4. (a) SEM image of sample with nominal composition $Zn_{0.999}Al_{0.001}O$ after thermal etching. Inset shows a possible precipitate of spinel phase formed at the grain boundaries. b) EDS analysis from regions (1) and (2), suggesting an Al-doped ZnO and spinel phase composition, respectively.

because of problems in the Al dispersion. However, the influence of the spinel phase on the thermoelectric properties will be neglected because its maximum concentration was only 3 vol% respect to the Al-doped ZnO phase, and no abnormal behavior in electric resistivity and Seebeck coefficient were observed (not shown).

Fig. 5a and b show the carrier concentration (n) and Hall mobility (μ) as a function of Al additive concentration, respectively. Carrier concentration and Hall mobility increase as the Al additive concentration rises due to the net increment of Al^{3+} dopant ions. According to a previous work, the maximum in carrier concentration observed in Fig. 5a could be explained, considering that at high additive concentrations, only a limited portion of the added Al might be effective as a dopant.[12]

Fig. 6 shows the carrier concentration as a function of *c*/*a* lattice ratio, indicating a non-linear behavior. As the ZnO lattice is compressed up to $c/a = 1.6014$, the carrier concentration slightly increases; however, at higher compressions of *c*/*a* ratio the carrier concentration rises up to a limit value of $1 \times 10^{20}\ cm^{-3}$. This tendency could be explained by the fact that as *c*/*a* achieves the maximum compression, the Al doping in the structure is geometrically restricted.

Fig. 7 shows the absolute value of Seebeck coefficient (α) as a function of carrier concentration. Seebeck coefficient increases as the carrier concentration decreases in agreement with the

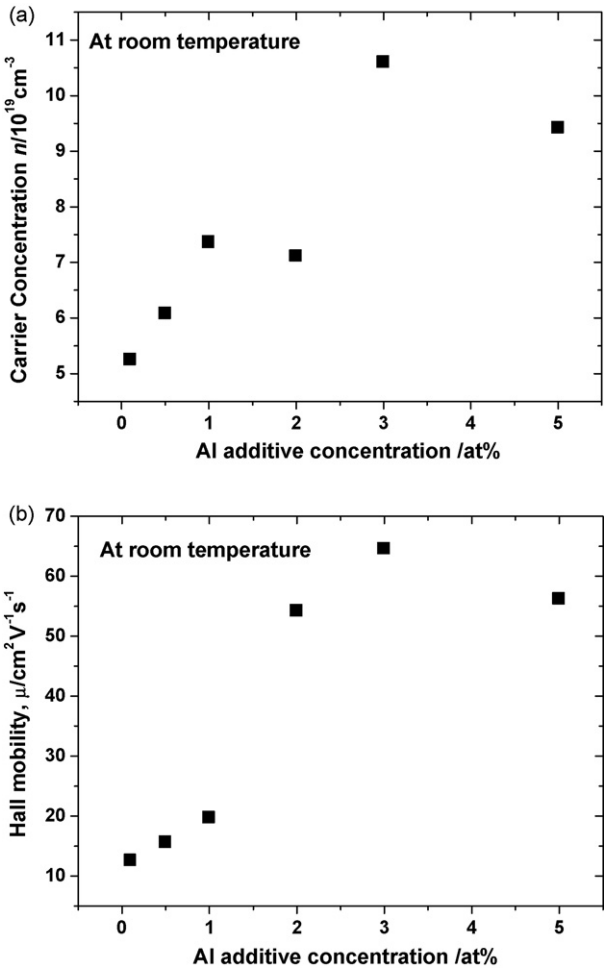

Fig. 5. Carrier concentration (n) and Hall mobility (μ) as a function of Al additive concentration at room temperature, respectively.

following model proposed by Jonker.[13]

$$\alpha = -\frac{k_B}{e}\left(\ln\left(\frac{N_c}{n}\right) + A\right) \quad (1)$$

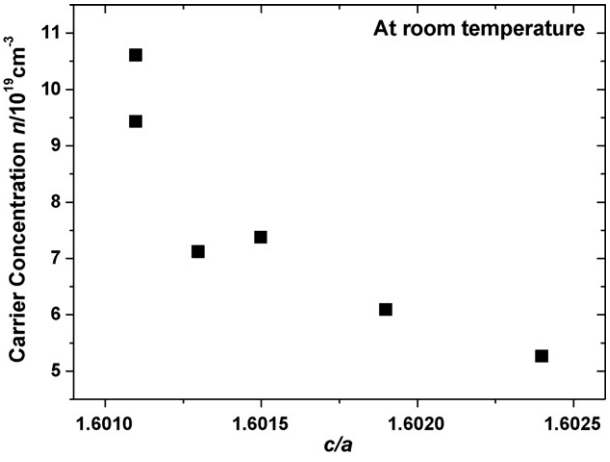

Fig. 6. Carrier concentration (n) as a function of c/a lattice ratio at room temperature. A limit value of carrier concentration of around $1 \times 10^{20}\,\mathrm{cm}^{-3}$ is achieved.

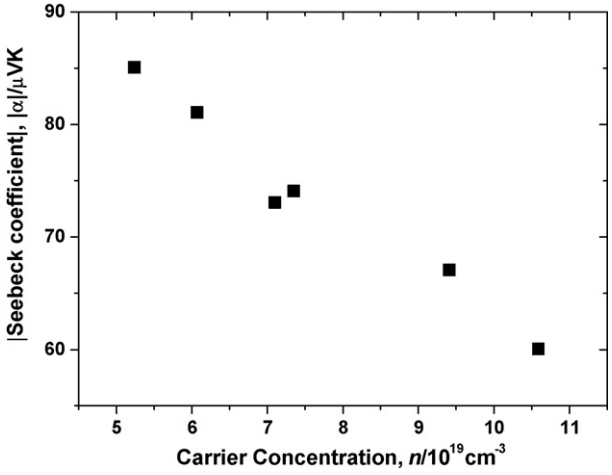

Fig. 7. Absolute value of Seebeck coefficient (α) as a function of carrier concentration (n).

where k_B is the Boltzmann constant, e is electron charge, N_c is the effective density of states, and A corresponds to a transport term; for simplicity, hereinafter A will be considered constant. Thus, the Seebeck coefficient depends on carrier concentration and effective density of states. The carrier concentration contribution to the thermoelectrical properties has been discussed in previous works;[2] however, the contribution of band structure, and subsequently electron effective mass (m^*), has not been exhaustively studied yet.

To evaluate the effective mass, the following equations are used:[14]

$$\alpha = -\frac{k_B}{e}\left(\frac{(r+2)F_{r+1}(\eta^*)}{(r+1)F_r(\eta^*)} - \eta^*\right) \quad (2)$$

where, $\eta^* = \eta/k_B T$ is the reduced Fermi level and F_r is the Fermi integral of order r.

$$F_r = \int_0^\infty \frac{x^r}{1+\exp^{(x-\eta^*)}}\mathrm{d}x \quad (3)$$

The parameter r is called scattering parameter and it depends on the scattering mechanism at a given temperature.[15] A reasonable value for r at room temperature can be assumed to be $r = 0.5$.[7] Additionally, a general expression for carrier concentration can be expressed as follows:[16]

$$n = 5.437 \times 10^{15}\left(\frac{m^*}{m_0}T\right)^{3/2}\int_0^\infty \frac{\varepsilon^{1/2}(1+\beta\varepsilon)^{1/2}(1+2\beta\varepsilon)}{1+\exp(\varepsilon-\eta^*)}\mathrm{d}\varepsilon \quad (4)$$

where β is a non-parabolic coefficient and m^* is the effective mass. The value for coefficient β will be assumed to be 0.1.

Fig. 8 shows the effective mass (m^*) as a function of c/a ratio. Effective mass was estimated by resolving numerically the Eqs. (2)–(4) at room temperature. The effective mass slightly increases from 0.27 to $0.30 m_0$ as the c/a ratio decreases (c-axis compression), apparently agreeing with the behavior predicted by Alahmed et al. in a previous first-principles simulation.[5]

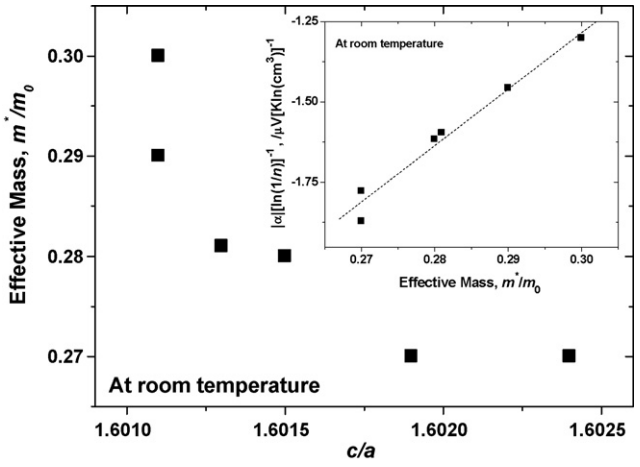

Fig. 8. Effective mass (m^*) as a function of c/a lattice ratio. Inset corresponds to absolute value of Seebeck coefficient at room temperature as normalized by $\ln(1/n)$ to cancel the carrier concentration (n) contribution.

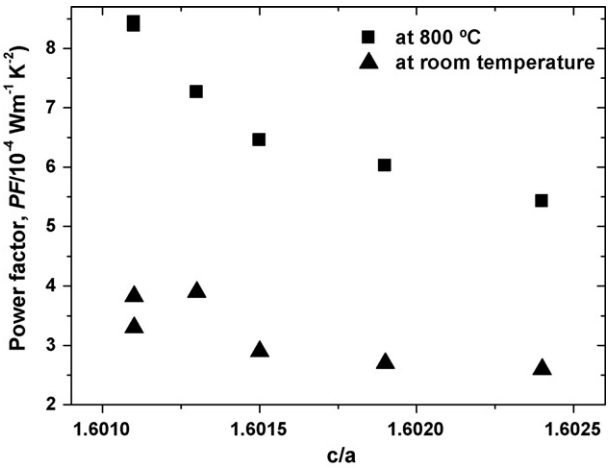

Fig. 10. Power factor (PF) as a function of c/a lattice ratio at room temperature and 800 °C. The maximum power factor increases from 3.9 to 8.5×10^{-4} $Wm^{-1}K^{-2}$ as the temperature rises from room temperature to 800 °C.

Besides, inset in Fig. 8 shows the absolute value of Seebeck coefficient at room temperature as a function of effective mass (m^*). According to Eq. (1), Seebeck coefficient is presented as normalized by $\ln(1/n)$ to cancel the carrier concentration contribution. Thus, as the lattice (c/a) is compressed, the effective mass increases and a net enhancement of Seebeck coefficient is induced. Unfortunately, effective mass variation is quite small, so it is hard to distinguish the contributions of lattice compression to the variation of effective mass from non-parabolicity of ZnO band structure. However, the effective mass increases only at high c/a lattice compression as it has been predicted by first-principles calculations.[5] suggesting that the c/a ratio could play a role in the enhancement of effective mass as it is suggested in Fig. 8.

Fig. 9 shows Hall mobility as a function of the effective mass. Considering Drude's formulation, Hall mobility could be expressed in terms of electron charge (e), carrier collision time (τ), and effective mass (m^*) as follows:[17]

$$\mu = \frac{e\tau}{m^*} \tag{5}$$

However, evidently, the tendency shown in Fig. 9 contradicts this equation. A possible explanation for this discrepancy in the Hall mobility behavior could be made by considering a model proposed by Srikant et al.[3]

In this model, the defects are mainly located at grain boundaries acting as carrier traps. Thus, a potential barrier will be induced at the grain boundary. The magnitude of this barrier depended on carrier concentration; this is because a significant proportion of total carriers will be trapped at the grain boundary at a low carrier concentration, reducing the apparent mobility through the material, and contrarily the proportion of total carriers trapped at the grain boundary decreases at a high carrier concentration and therefore the apparent mobility should increase. Thus, Hall mobility is mainly affected from carrier traps at grain boundaries than change in effective mass or c/a lattice ratio.

Fig. 10 shows power factor as a function of c/a ratio for sintered Al-doped ZnO samples measured at room temperature and 800 °C. The highest power factor is achieved at the highest c/a compressions, 3.9 to 8.5×10^{-4} Wm^{-1} K^{-2}, at room temperature and 800 °C, respectively. A change in the slope is observed around $c/a = 1.6014$, suggesting that a high c/a compression is required to enhance the power factor.

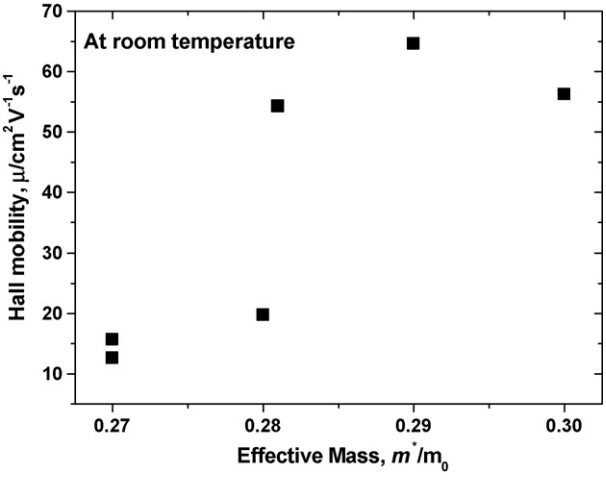

Fig. 9. Hall mobility (μ) as a function of effective mass (m^*) at room temperature.

4. Conclusion

Sintered $Zn_{1-x}Al_xO$ samples with $x = \{0.001, 0.005, 0.01, 0.02, 0.03, \text{or } 0.05\}$ were thermoelectrically characterized from room temperature up to 800 °C. The lattice parameter ratio c/a was used to propose an explanation of doping effect on the Seebeck coefficient, effective mass, and power factor behaviors. As the doped ZnO lattice is compressed along the c-axis, the effective mass (m^*) slightly increases, enhancing its net con-

tribution to the Seebeck coefficient. In particular, the effective mass dependence with *c*/*a* lattice ratio seems to be in agreement with the previous first-principles simulation.[5]

Additionally, the results suggested that the maximum carrier concentration should be limited by high *c*/*a* compressions, whereas the Hall mobility is mainly affected by the change in microstructure or defects. A correlation between *c*/*a* lattice ratio and the maximum power factor for this kind of ceramics ($8.5 \times 10^{-4}\,\mathrm{Wm^{-1}K^{-2}}$ at 800 °C) was also found. Finally, the results suggest that in ion-doped ZnO system, a high compression of *c*/*a* ratio due to heavy doping could be a key to improve the power factor.

Acknowledgment

The authors sincerely thank Dr. I. Matsubara and Dr. W.-S. Shin of AIST for their help during experimentation.

References

1. Ohtaki, M., Tsubota, T., Eguchi, K. and Arai, H., High-temperature thermoelectric properties of $(Zn_{1-x}Al_x)O$. *J. Appl. Phys.*, 1996, **79**(3), 1816–1818.
2. Kinemuchi, Y., Ito, C., Kaga, H., Aoki, T. and Watari, K., Thermoelectricity of Al-doped ZnO at different carrier concentrations. *J. Mater. Res.*, 2007, **7**(22), 1942–1946.
3. Srikant, V., Sergo, V. and Clarke, D., Epitaxial aluminum-doped zinc oxide thin films on sapphire. II. Effect of substrate orientation. *J. Am. Ceram. Soc.*, 1995, **78**(7), 1935–1939.
4. Özgür, Ü., Alivov, Y., Liu, C., Teke, A., Reshchikov, M., Doğan, S., Avrutin, V., Cho, S. and Morkoç, H., A comprehensive review of ZnO materials and devices. *J. Appl. Phys.*, 2005, **98**, 041301.
5. Alahmed, Z. and Fu, H., Polar semiconductor ZnO under inplane tensile strain. *Phys. Rev. B*, 2008, **77**, 045213.
6. Singh, A., Mehra, E., Yoshida, A. and Wakahara, A., Doping mechanism in aluminum doped zinc oxide films. *J. Appl. Phys.*, 2004, **95**(7), 3640–3643.
7. Young, D., Coutts, T., Kaydanov, V., Gilmore, A. and Mulligan, W., Direct measurement of density-of-states effective mass and scattering parameter in transparent conducting oxides using second-order transport phenomena. *J. Vac. Sci. Technol. A*, 2000, **18**(6), 2978–2985.
8. Rupp, B., XLAT—least squares refinement of cell constants. *Scripta Metall.*, 1988, **22**, 1.
9. Powder Diffraction Files, The International Centre for Diffraction, Swarthmore, USA, 2004.
10. Shirouzu, K., Ohkusa, T., Hotta, M., Enomoto, N. and Hojo, J., Distribution and solubility limit of Al in Al_2O_3-doped ZnO sintered body. *J. Ceram. Soc. Jpn.*, 2007, **115**(4), 254–258.
11. Cai, K., Müller, E., Drasăr, C. and Mrotzek, A., Preparation and thermoelectric properties of Al-doped ZnO ceramics. *Mater. Sci. Eng. B*, 2003, **104**, 45–48.
12. Tsubota, T., Ohtaki, M., Eguchi, K. and Arai, H., Thermoelectric properties of Al-doped ZnO as a promising oxide material for high temperature thermoelectric conversion. *J. Mater. Chem.*, 1997, **7**(1), 85–90.
13. Jonker, G., The application of combined conductivity and Seebeck-effect plots for the analysis of semiconductor properties. *Phillips Res. Rep.*, 1968, **23**, 131–138.
14. Fistul, V. I., *Heavily Doped Semiconductors*. Plenum, New York, 1969, p. 51–55.
15. Durcsewski, K. and Ausloos, M., Nontrivial behavior of the thermoelectric power: electron–electron versus electron–photon scattering. *Phys. Rev. B*, 2000, **61**(8), 5303–5310.
16. Bhan, R. and Dhar, V., Carrier density approximation for non-parabolic and highly degenerated HgCdTe semiconductors. *Semicond. Sci. Technol.*, 2004, **19**(3), 413–416.
17. Ashcroft, N. and Mermin, N., *Solid State Physics*. Thompson Learning, USA, 1976, p. 601–602.